Experimental Evidence for the Pressure Dependence of the Reaction Rate Constant between Acetic Acid and Hydroxyl Radicals

Yi-wen Huang,*,† Timothy J. Dransfield,‡ and James G. Anderson†

Department of Chemistry and Chemical Biology, Harvard University, 12 Oxford Street, Cambridge Massachusetts 02139, United States, and Department of Chemistry, University of Massachusetts—Boston, 100 Morrissey Boulevard, Boston Massachusetts 02125, United States

Received: July 12, 2010; Revised Manuscript Received: September 17, 2010

The reaction rate constant of acetic acid with the hydroxyl radical is measured at 93 Torr with our high-pressure flow system (HPFS) and found to display a negative temperature dependence that can be described by the Arrhenius expression, $k(T) = (2.44 \pm 0.22) \times 10^{-14} \exp((1027 \pm 24)/T))$ cm^3 molecule^{-1} s^{-1}. Compared with our previously reported 7 Torr data, we find a noticeable pressure dependence. This dependence is observed to increase with decreasing temperature. This finding is consistent with a termolecular reaction mechanism. It is the first experimental evidence of the pressure dependence for this rate constant. A kinetics model is constructed, and the model results agree qualitatively with our experimental data. The extrapolated rate constant of the title reaction would be faster than previously believed at conditions of the upper troposphere/lower stratosphere, suggesting that the importance of acetic acid in its impact on HO_x chemistry is currently underestimated.

Introduction

A recent report[1] on a small but noticeable increase of methane concentrations and its attribution to a potentially small decrease of OH concentrations highlights the importance of understanding the HO_x chemistry in the upper troposphere/lower stratosphere (UTLS) region. Tropospheric HO_x and OH concentrations are crucial to determining the lifetimes of important volatile organic compounds, including methane, and need to be understood fully. However, in situ observations of HO_x do not agree well with existing model simulation results,[2] indicating a need to seek potential HO_x sources in the UTLS region. The reaction between OH and CH_3COOH has been a topic of interest due to the large quantity of acetic acid observed in the atmosphere,[3] its kinetics, complex reaction mechanisms,[4−8] and unusual potential energy surface (PES).[9,10] The OH + CH_3COOH reaction generates HO_x and has the potential of becoming an important HO_x source in the UTLS region.

Most of the experimental kinetics studies agreed that the rate constant exhibits a negative temperature dependence.[5−8,11] Butkovskaya et al.[6] and De Smedt et al.[9] experimentally measured the prompt yield of CO_2 and reported that the there are two product channels: channel 1a where OH abstracts the carboxylic hydrogen via a complex formation to produce CO_2 as the prompt product and channel 1b which results in CH_2COOH radical formation, and the branching ratio of channel 1a versus 1b is roughly 2:1 at room temperature. Under NO_x-rich conditions, channel 1a is a HO_x source, as the methyl radical generated rapidly undergoes oxidation by the addition of diatomic oxygen to form the methylperoxy radical. In the presence of NO, this species forms methoxy, which subsequently reacts again with oxygen to yield formaldehyde and an HO_2 radical. In NO_x-poor conditions, channel 1a is not a HO_x source. Meanwhile, channel 1b is a net HO_x source independent of NO_x conditions.[6] At temperatures below 295 K, however, there is only one reported data point by Butkovskaya et al.[6] that suggested an unchanged 2:1 branching ratio for the two channels.

$$CH_3COOH + OH \rightarrow CH_3COO + H_2O \rightarrow CH_3 + CO_2 + H_2O \quad (1a)$$

$$\rightarrow CH_2COOH + H_2O \quad (1b)$$

The experimental study by Khamaganov et al.[8] suggested that channel 1b proceeds via a direct H-abstraction mechanism and exhibited a positive temperature dependence at temperatures above 515 K. Singleton et al.[5] and Vimal and Stevens[7] reported a significant decrease in reaction rate upon deuteration of the carboxylic hydrogen, which suggested that tunneling could play an important role in the step following complex formation in channel 1a.[7]

The two-channeled PES of the reaction of OH + CH_3COOH is shown in Figure 1 using energies reported by Rosado-Reyes and Francisco.[10] Both De Smedt et al.[9] and Rosado-Reyes and Francisco[10] investigated the PES using Gaussian, and their results are quite similar. The well depth of channel 1a was calculated to be 6.5 and 4.4 kcal mol^{-1} for channel 1b by Rosado-Reyes and Francisco.[10] After the complexes form, the barrier heights for channel 1a and channel 1b are 2.1 and 4.0 kcal mol^{-1} above the reactants. $CH_3COOH-OH^*$ denotes the excited complex, whereas $CH_3COOH-OH$ is the thermalized complex. Rosado-Reyes and Francisco[10] suggested that the initial steps in both channels involve complex formation, whereas the study by De Smedt et al.[9] focused on channel 1a and did not suggest a mechanism for channel 1b. Though tunneling is thought to play a role in overcoming the barriers to proceed to products, it was not well accounted for and may be underestimated.[7,9]

* To whom correspondence should be addressed. E-mail: ywhuang@huarp.harvard.edu.
† Harvard University.
‡ University of Massachusetts—Boston.

10.1021/jp106446q
Published on Web 10/06/2010

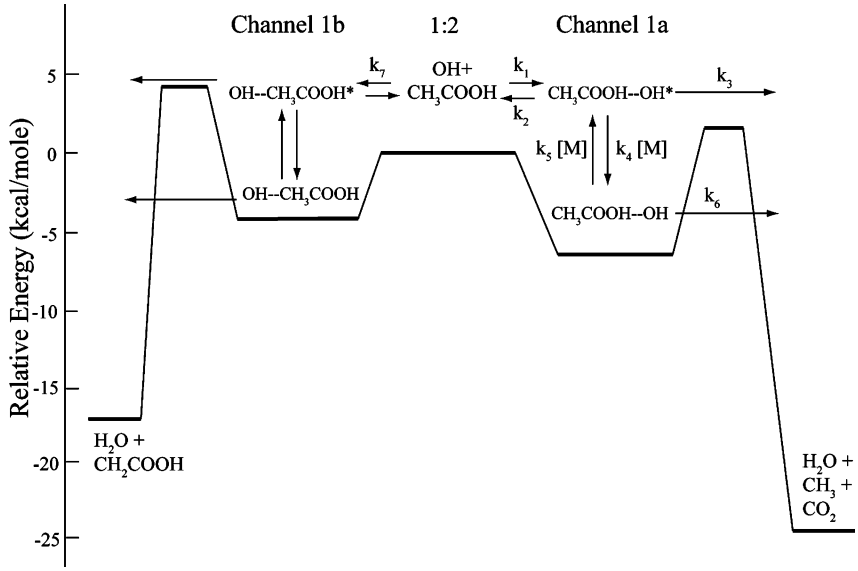

Figure 1. Potential energy surface for OH + CH_3COOH. The relative energies are calculated by Rosado-Reyes and Francisco.[10] Channel 1a is the main channel via a complex formation mechanism, leading to prompt CO_2 production, whereas channel 1b has a shallower well and leads to H_2O + CH_2COOH. The rates k_1-k_7 are used in a kinetics model described in the Results and Discussions section.

Sun and Sayes took into account the tunneling factor, and the calculated rate coefficients agreed with the experimental values better.[12] A reaction rate involving complex formation as a first step is accompanied by a negative temperature dependence and a positive pressure dependence if the ratio of the rate constant to form products to that for reversion to products decreases as temperature increases. This usually occurs when the barrier to products is lower than the energy of the reactants and the density of states at that barrier is lower than the density for reversion to products. In the case studied here, even though the barrier to products is higher than the energy of the reactants, tunneling through that barrier effectively renders it lower.

The concentration of bath gas molecules ([M]) determines how much of the excited $CH_3COOH-OH^*$ complex is collisionally stabilized. The stabilization enhances the reaction rate, and increasing pressure results in faster reaction rate.

There have been limited reports on the pressure dependence of this rate constant. Khamaganov et al.[8] measured the reaction rate at 50 and 100 Torr, from 287 to 802 K, and reported no noticeable pressure dependence. Vimal and Stevens[7] compared their data at 2−5 Torr and 263−373 K with those of Butkovskaya et al.[6] at 200 Torr and 229−300 K and Singleton et al.[5] at 500 Torr and 297−446 K, found that there was no significant difference in the three data sets, and concluded that there is no pressure dependence in this rate constant.

Previously, we reported a kinetics data set at 7 Torr from 255 to 355 K using our high-pressure flow system (HPFS).[11] Our data confirmed a negative temperature dependence for the reaction rate of OH + CH_3COOH. An Arrhenius expression of $k(T) = (5.38 \pm 0.28) \times 10^{-14} \exp(740 \pm 51/T)$ cm^3 molecule^{-1} s^{-1}, corresponding to a negative activation energy of ∼−1.5 kcal/mol, with $k = (6.77 \pm 0.14) \times 10^{-13}$ cm^3 molecule^{-1} s^{-1} at 293 K, was obtained. At temperatures below 300 K, dimerization of acetic acid became an experimental challenge. Though acetic acid dimer is much less reactive toward OH due to the lack of sites for hydrogen bonding to make a dimer−OH complex,[5,6] making it insignificant in determining the rate constant of OH reacting with acetic acid monomer, its presence complicates the quantification of acetic acid monomer at low temperatures. While all other studies[6−8] relied on an expression for the dimer/monomer equilibrium constant to deduce the acetic acid monomer concentration and introduced large uncertainty to the reaction rate at low temperatures, our direct detection of acetic acid monomer using FTIR enabled us to reduce uncertainty in our data at low temperatures. The IR spectra were treated with a mathematical filter to remove the acetic acid dimer feature for speedy analysis of the experimental data.

With slight modification to the instrument, we are able to obtain a kinetics data set for the title reaction at 93 Torr and 241−301 K. Comparison of our 7 and 93 Torr data reveals a noticeable pressure dependence that increases with decreasing temperature. This is the first time the pressure dependence is observed experimentally for the reaction of OH and CH_3COOH. A kinetics model using parameters reported by Vimal and Stevens[7] is constructed, and its result agrees reasonably well with our experimental data.

Experimental Section

Harvard's HPFS has been described previously in the literature,[11,13−16] including recent experiments on the temperature dependence of the kinetics of OH + CH_3COOH at 7 Torr.[11] In the 7 Torr experiments, H + NO_2 → OH + NO was used as the OH source. The carrier flow was nitrogen and pumped out after passing through the detection zone once. Acetic acid was purified and transferred to a glass bulb filled with nitrogen to make a 2% bulb for injection through the excess reagent manifold near the carrier flow injection site. To ensure that systematic error is minimized, the reaction rate of OH + ethane and/or OH + cyclohexane was measured prior to making the OH + CH_3COOH measurements.

To perform kinetics at pressures higher than 15 Torr and maintain a nontransitional flow profile, modifications to the instrument are required and described below. A roots blower in the return line is used to increase the velocity. The carrier flow is 200 slm to reach pressures above 25 Torr. The flow conditions at 93 Torr are turbulent (the Reynolds numbers are >10 000), and the velocity is around 16−21 m/s. An electronic valve controls the opening to the pump line and is partially open to allow only a fraction of the carrier flow to be pumped out of the system to sustain the pressure. This configuration results in recirculation of the carrier flow, and the majority of the carrier

flow and acetic acid passes the detection zone multiple times. Kinetics data are taken when acetic acid concentration reaches steady state. The OH radicals, however, do not survive beyond one pass. The recirculation mode results in a partial flushing of the excess reagent, and the more acetic acid that is injected, the longer it takes for the system to clear all of the acetic acid. Thus, the run time for each experiment at 93 Torr is prolonged to ~30 min. It has been established that the different flow conditions, laminar or turbulent, do not affect measured rates of OH + ethane and OH + cyclohexane,[13,14] and our measurements of OH + ethane and OH + cyclohexane agree with previous measurements to within 5%.[16] The lengthened run time only makes the high-pressure experiments more challenging since everything, from the radical source to reaction temperature, has to remain unchanged for the duration of the run.

In the previous study,[11] OH radicals were generated by $H + NO_2 \rightarrow OH + NO$. In the higher pressure conditions presented in this paper, the increase in carrier flow calls for larger flows of both OH radicals and acetic acid. However, if OH is generated via $H + NO_2 \rightarrow OH + NO$, elevated flows of NO_2 could lead to reactions of OH with NO and NO_2 and cause undesired OH regeneration or loss. To overcome this, OH radicals in the present work are instead generated via the $F + H_2O \rightarrow HF + OH$ reaction. The measured rate coefficients of OH + ethane and OH + cyclohexane using the $F + H_2O$ radical source are the same as those measured using $H + NO_2$ as the radical source, suggesting that the source change does not affect kinetics results. A 1% mixture of fluorine in argon is sent through the microwave-induced plasma to generate fluorine atoms. The fluorine atoms quickly react with water vapor introduced through the side arm of the injector. The inside of the quartz injector is coated with halocarbon wax to minimize OH loss to the injector wall. Once injected into the system, OH is detected via laser-induced fluorescence (LIF). There are no background OH counts when fluorine is not added to the flow, confirming that all OH is produced via the $F + H_2O \rightarrow OH + HF$ reaction. Due to the high dissociation efficiency of the plasma, only a flow of 2 sccm or less is needed for fluorine. The argon flow, however, is much greater in order to expedite the injection of OH radicals, usually close to 2 slm. The water vapor flow is usually 20 sccm to ensure complete conversion of fluorine atoms. The overall flow from the radical source is no more than 1% of the total flow.

Acetic acid concentrations are quantified with a White cell coupled to an FTIR spectrometer. The path length is calibrated with a known mixture of dichlorodifluoromethane (F12) in nitrogen and cross-checked with long-path UV absorption. In our 7 Torr experiments, the acetic acid was injected from a 12 L glass bulb filled with nitrogen gas saturated with acetic acid at room temperature. The 93 Torr experiments last longer and require more acetic acid than the glass bulb can provide to achieve more than a 1 order of magnitude decay. Therefore, for the highest concentrations of acetic acid, a different method for acetic acid injection is used. After acetic acid is first purified using several freeze−pump−thaw cycles, it is transferred into a two-neck glass flask. A nitrogen flow is then passed over the liquid acetic acid to carry the vapor into the flow system through a loop-shaped injector 4.5 m upstream of the radical injection site. This setup allows for continuous flow of acetic acid and can provide higher concentrations of acetic acid than the glass bulb. The disadvantage is that this injection site requires manual operation to modulate the flow, further prolonging the run time. It is only used for some of the highest concentration points at temperatures below 265 K.

TABLE 1: Summary of All Experimental Conditions at 93 ± 3 Torr

temp (K)	[acetic acid] (10^{13} molecules cm^{-3})	rate constant (k) (10^{-13} cm^3 molecule^{-1} s^{-1})	no. of experiments
241	0.16−3.28	17.6 ± 1.0	4
249	0.75−4.21	14.9 ± 1.0	6
269	1.86−8.42	11.0 ± 0.5	5
301	3.11−11.4	7.41 ± 0.2	5

We described our data analysis methodology in our previous paper.[11] While we could fit the acetic acid spectrum using two different methods, a simultaneous fitting method and a filter method, we opted for the filter method since it is faster and yields results that are in excellent agreement with the simultaneous fitting method (within 3%) in the 7 Torr study. In our current study, at the coldest temperatures, acetic acid dimer concentrations are comparable to the monomer concentrations, causing the baseline of the monomer spectral feature to shift up slightly. The disagreement between the two spectral analysis methods increases to 7% in our data below 245 K. At temperatures above 245 K, the two methods disagree by no more than 3%. Therefore, the error at the coldest temperature is slightly greater than all others. The main source of uncertainty in our high-pressure data is from the FTIR spectrometry, and we estimate an 8% error at room temperature and 13% error at the lowest temperature. In 7 Torr experiments, the pitot tube reading of the flow velocity introduced larger uncertainty when acetic acid was injected and disturbed the bulk flow. In the 93 Torr experiments, injection of acetic acid no longer presents a problem because the carrier flow is much greater than that in 7 Torr experiments. The pitot tube no longer senses the disturbance caused by introduction of acetic acid to the system. The 2σ errors are estimated to be ~10% at room temperature and ~15% at the lowest temperature.

Results and Discussion

Rate Constant of OH + CH_3COOH at 93 Torr. Table 1 summarizes the experimental conditions and results. The rate constants from individual runs are binned and averaged according to temperature. All experiments were performed between 90 and 96 Torr under pseudo-first-order conditions, with OH being the limiting reactant and acetic acid in excess. The OH decay monitored in our system can be described as follows

$$[OH]_{\text{axis } n(n=2-5)} = [OH]_{\text{axis 1}} \times \exp(-k \times \text{time} \times [\text{acetic acid}]) \quad (2)$$

Figure 2 illustrates a pseudo-first-order decay of OH with various acetic acid concentrations at all axes, normalized with respect to axis 1. The decay in the logarithm of the OH concentration is typically linear over 1−1.5 orders of magnitude after subtraction of laser scatter. The initial OH concentrations are ~10^9 molecules cm^{-3}. The second-order rate constant of the OH + CH_3COOH reaction at 293 K and 93 Torr is (7.93 ± 0.15) × 10^{-13} cm^3 molecule^{-1} s^{-1}. Figure 3 shows all the raw data, 93 Torr data in red dots with a dashed fit line and 7 Torr data in black dots with a black fit line. The Arrhenius expression at 93 Torr from the weighted fit is $k(T) = (2.44 \pm 0.22) \times 10^{-14} \exp((1027 \pm 24)/T)$. At 293 K, the rate constant at 7 Torr was measured to be 6.77 × 10^{-13} cm^3 molecule^{-1} s^{-1} in our system. In comparison with the rate measured at 293 K and 93 Torr, 7.93 × 10^{-13} cm^3 molecule^{-1} s^{-1}, the difference

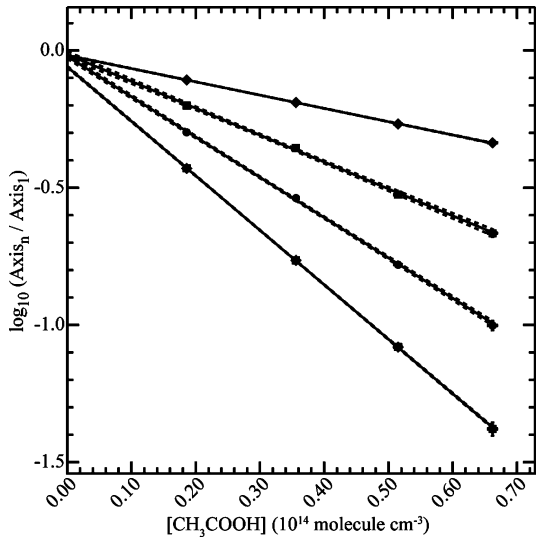

Figure 2. Sample first-order decay plot for the OH signals at 269 K and 94 Torr. Different lines represent different LIF detection axes, with the line through the diamonds being the second axis, etc. Note that our *x* axis is the acetic acid concentration and that this is a relative decay with respect to detection axis 1. The resulting rate constant is 11.8×10^{-13} cm^3 molecule^{-1} s^{-1} at 269 K and 94.0 Torr.

in pressure gives rise to a 20% increase at 293 K. At 240 K, the difference in rate constant is elevated to ~50%, with 11.7×10^{-13} cm^3 molecule^{-1} s^{-1} at 7 Torr and 17.6×10^{-13} cm^3 molecule^{-1} s^{-1} at 93 Torr. There is a detectable pressure dependence in the rate constant, along with a negative temperature dependence. The OH + ethane and/or OH + cyclohexane measurements exhibit no pressure dependence, despite the order-of-magnitude pressure change. This provides assurance that there is no systematic error or drift contaminating this data set and that this is in fact a real pressure dependence in the rate constant of OH + CH_3COOH.

Our fit result of $(2.44 \pm 0.22) \times 10^{-14}$ exp $((1027 \pm 24)/T)$ cm^3 molecule^{-1} s^{-1} corresponds to a negative activation energy of ~2 kcal mol^{-1}, which is ~0.5 kcal mol^{-1} larger than the negative activation energy found in our previous 7 Torr study.[11] This suggests that increasing pressure effectively deepens the well by collisionally stabilizing the prereactive $CH_3COOH-OH$ complex, elevating the overall rate.

Figure 4 summarizes all existing data on the title reaction rate. Prior to this study it was thought that there was no pressure dependence in this rate constant, and the rate constant might have reached the high-pressure limit even at 7 Torr.[7,11] Though recent studies from Butkovskaya et al.,[6] Vimal and Stevens,[7] Khamaganov et al.,[8] and Huang et al.[11] agree within experimental error, disparity still exists. With the addition of our 93 Torr data set and the knowledge that the pressure dependence does exist, it is not surprising that our 93 Torr data agree better with the data of Butkovskaya et al.[6] at 200 Torr than with other data sets at lower pressures and that our 7 Torr data agree better with those of Vimal and Stevens[7] at 2−5 Torr.

Impact of K_{eq} Expression on the Rate. While we use FTIR spectrometry to directly measure the acetic acid monomer concentration and do not rely on the equilibrium constant to deduce the acetic acid monomer concentration, three of the temperature-dependent studies do.[6−8] As pointed out in our previous paper,[11] the equilibrium constant expression directly impacts the acetic acid monomer concentration, which consequently affects the rate constant. Butkovskaya et al.[6] used UV single-wavelength absorption spectroscopy to constrain the acetic acid monomer concentration, coupled with an equilibrium constant expression of 2.8×10^{-8} exp$(7290/T)$. Vimal and Stevens[7] used a different expression of 7.1×10^{-9} exp$(7705/T)$, and Khamaganov et al.[8] derived yet another expression of $\ln(K_{eq}) = -18.07 + (7522/T)$. Due to the exponential nature of the equations, employing different expressions results in K_{eq} numbers that are drastically different at temperatures below 300 K. We follow the procedure by Butkovskaya et al.[6] to calculate a monomer concentration using ln (Trans) $= L(1.35 \times 10^{-19}$ [monomer] $+ 1.84 \times 10^{-19}$ [dimer]), where Trans is the transmittance of the beam light and L is the length of the optical path. Coupled with an expression for K_{eq}, we determine the acetic acid monomer concentration. Figure 5 demonstrates all the results from this calculation using three different K_{eq} expressions reported assuming Trans $= 1\times 10^{-2}$ to 1×10^{-4}. Mb denotes the acetic acid monomer concentration obtained using the K_{eq} expression from Butkovskaya et al.,[6] Mv is the monomer concentration calculated using K_{eq} in Vimal and Stevens,[7] and Mk is from using the expression derived by Khamaganov et al.[8] The dotted lines represent a transmittance of 1×10^{-4}, the dashed lines represent a transmittance of $1\times$

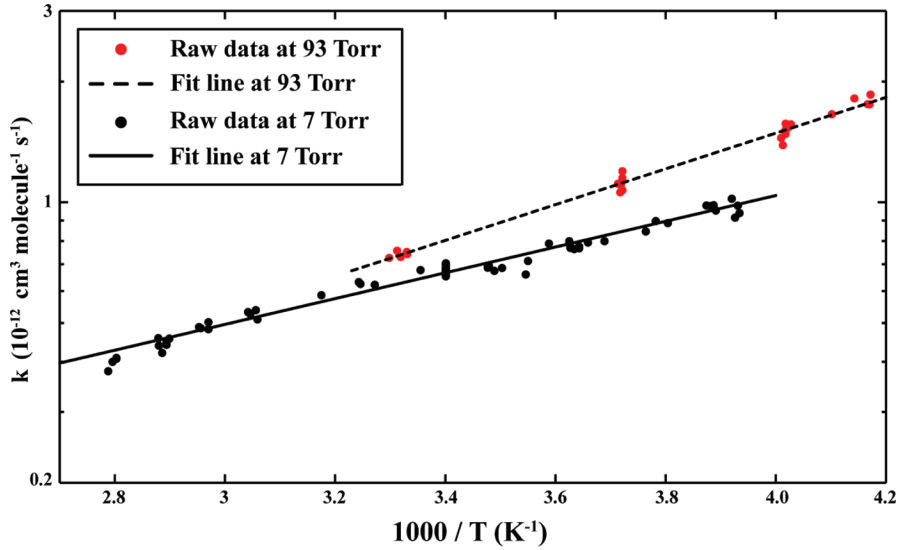

Figure 3. Comparison of raw data at 93 and 7 Torr and their respective weighted fits. The Arrhenius expression at 7 Torr is $(5.38 \pm 0.28) \times 10^{-14}$ exp $((740 \pm 51)/T)$ cm^3 molecule^{-1} s^{-1}, and the Arrhenius expression at 93 Torr is $(2.44 \pm 0.22) \times 10^{-14}$ exp $((1027 \pm 24)/T)$ cm^3 molecule^{-1} s^{-1}.

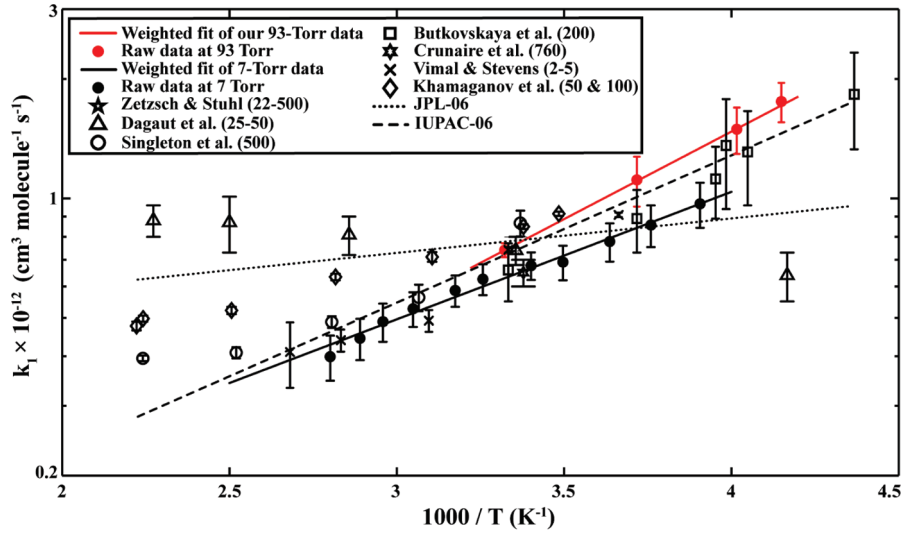

Figure 4. Summary of all experimental data, their errors, and the fits recommended by JPL and IUPAC. The numbers in parentheses in the legend are the pressures for each experiment in Torr. The red solid line is our fit to our data at 93 Torr. The black solid line is our fit to our data at 7 Torr. The dashed line is the IUPAC-06 recommendation. The dotted line is the JPL-06 recommendation.

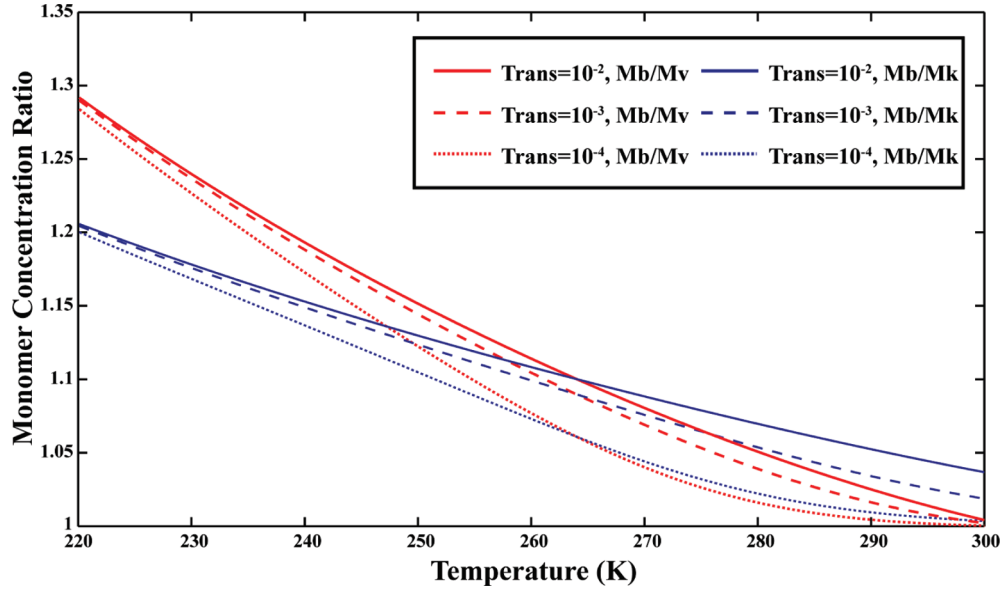

Figure 5. Acetic acid monomer concentration comparison. Following the procedure of Butkovskaya et al.,[6] with different K_{eq} expressions, the acetic acid monomer concentrations are calculated with transmittance from 10^{-2} to 10^{-4}. Mb denotes the monomer concentration obtained using K_{eq} used by Butkovskaya et al.,[6] Mv is the monomer concentration calculated using K_{eq} employed by Vimal and Stevens,[7] and Mk is the calculated monomer concentration using K_{eq} derived by Khamaganov et al.[8] The lines are ratios of Mb/Mv and Mb/Mk to demonstrate that the monomer concentration can be different by 20−30% if different K_{eq} expressions are used at 220 K.

10^{-3}, and the solid lines are calculated with a transmittance of 1×10^{-2}. The red lines are from Mb/Mv, and the blue lines are from Mb/Mk. As clearly seen in Figure 5, when using K_{eq} from Butkovskaya et al.,[6] the acetic acid monomer concentration is about ~30% higher than if one used the K_{eq} from Vimal and Stevens[7] at 220 K and ~20% higher than using K_{eq} used by Khamaganov et al.[8] A higher acetic acid monomer concentration results in a lower estimate for the rate constant. Therefore, the rate constants reported by Butkovskaya et al.[6] could be underestimated by at least 20% at 220 K. At 247 K, the difference is roughly 10−15%. Increasing the 247 K data point reported by Butkovskaya et al.[6] by 15% gives a rate of 15.0×10^{-13} cm^{-3} molecule^{-1} s^{-1}, which is as high as our number at 248 K, 14.9×10^{-13} cm^{-3} molecule^{-1} s^{-1}. Thus, the discrepancy between our data here and those reported by Butkovskaya et al.[6] could be explained by potential error introduced by the K_{eq} expression used to quantify the acetic acid monomer concentration. Nonetheless, the data by Butkovskaya et al.[6] at 200 Torr agree better with our 93 Torr data than our 7 Torr data.

Kinetics Model Results and Comparison with Experimental Data. Starting with the assumption that k_1 is similar to that for the OH + acetone reaction, 2.67×10^{-11} cm^3 molecule^{-1} s^{-1}, Vimal and Stevens[7] used RRKM theory to calculate the temperature-dependent equilibrium constant for complex formation (OH + $CH_3COOH \leftrightarrow OH{-}CH_3COOH$) and determined the temperature-dependent k_2 at various temperatures. They also calculated $K_{eq} = k_4/k_5$ using RRKM theory. Vimal and Stevens[7] used the three-parameter expression for the overall rate constant of Butkovskaya et al.[6] and derived k_3 and k_6. In an effort to make qualitative connection between experimental data and theory, we constructed a kinetics model in Matlab using the rate constants reported by Vimal and Stevens[7] and compared the model results with our raw decay data. Table 2 lists all the parameters used in the kinetics model. We compare our 7 Torr

TABLE 2: Parameters Used in the Kinetics Model[a]

	temp (K)	k_1 (10^{11})	k_2 (10^8)	k_3 (10^6)	k_4/k_5 (10^5)	k_6 (10^2)	k_7 (10^{-13})	k_{total} (10^{-13})	k_{exp} (10^{-13})
Vimal and Stevens (base case)	300	2.67	2.5	4.2	0.3	0.8	N/A	6.8 (L), 7.9 (H)	6.7 (L), 7.4 (H)
best case	300	2.67	2.5	4.2	0.3	1.8	2.2	6.8 (L), 8.4 (H)	6.7 (L), 7.4 (H)

[a] L denotes the 7 Torr case, and H denotes the 93 Torr case. k_{total} is calculated using eq 2. k_{exp} denotes the experimentally measured rate for the reaction.

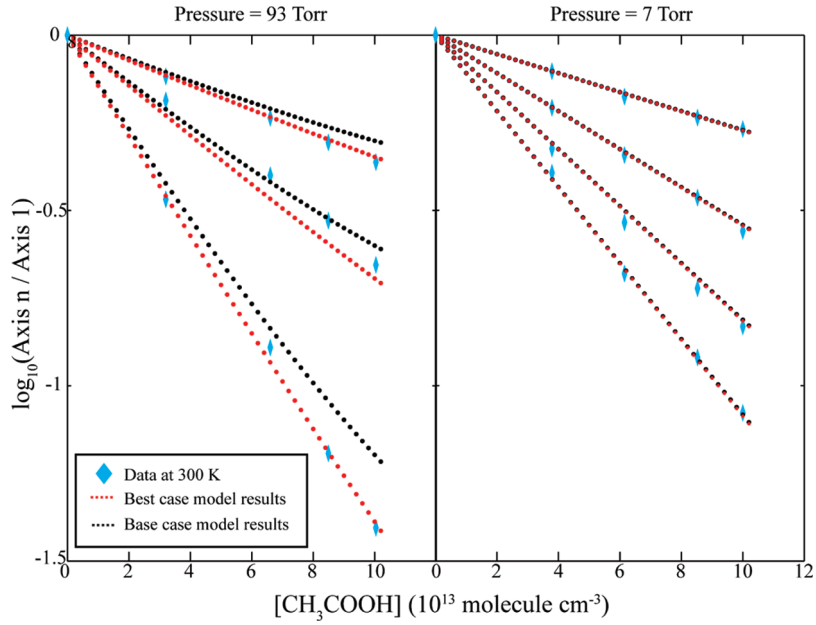

Figure 6. Comparison of model result and experimental data at 300 K using parameters in Table 2. The blue diamonds are raw decay data points from runs at 7 and 93 Torr. The black dots are simulations results using base-case parameters. The red dots are simulation results using best-case parameters.

data and 93 Torr data at 300 K using rate constants estimated by Vimal and Stevens at 300 K. In our 93 Torr data, data points of axis 4 are taken out due to laser misalignment. In an effort to depict the full two-channeled picture, we add a rate of $k_7 = 2.2 \times 10^{-13}$ (one-third of the rate of 6.7×10^{-13} at 300 K and 7 Torr) to account for channel 1b at room temperature. Note that Vimal and Stevens[7] did not report a k_7. The blue diamonds in Figure 6 are raw data from our decay plots. The black dots are model results using exactly the same parameters as those reported by Vimal and Stevens,[7] labeled as "base case". Though the agreement between the experimental data and the base-case model results is fair, we used the least-squares method to find the "best-case" parameters and plotted the results in red dots. The only parameter that required modification was k_6, and it was increased from 0.8 to 1.8×10^2. The "best-case" model results and experimental data agree better than the "base case". Not surprisingly, the two sets of parameters do not affect results at 7 Torr as much since pressure does not enhance the reaction rate as much as in the 93 Torr case. It should be noted that the uncertainties in the rate constants estimated by Vimal and Stevens,[7] though not explicitly reported, are not negligible. Thus, this exercise of making a connection between theoretically evaluated parameters and our experimental data is not meant for a quantitative comparison. Nonetheless, the kinetics model results demonstrate the point that the pressure dependence can be present in such PES. The overall rate expression of channel 1a can be described as the following[17]

$$k = k_1\left\{1 - k_2\left(k_2 + k_3 + \frac{k_6 k_4[M]}{k[_5M] + k_6}\right)^{-1}\right\} \qquad (3)$$

Combining the rates from both channels 1a and 1b, the overall rates from the kinetics model agree with experimental results.

Pressure Dependence of a Similar System. The pressure dependence of the rate constant of OH + CH_3COOH has never been observed experimentally. The strong negative temperature dependence found in the rate constant suggested a hydrogen-bonded complex formation mechanism that would be expected to have a positive pressure dependence associated with it. However, all the existing experimental data overlapped within experimental errors, and this led to the conclusion that there may not be a pressure dependence or that the reaction may have reached the high-pressure limit at pressures as low as 2−5 Torr.[7,11] The reaction of OH + HNO_3 has a potential energy surface similar to that of OH + CH_3COOH, and its rate constant was found to have not only a negative temperature dependence but also a positive pressure dependence that gets more pronounced as temperature decreases.[17−19] The expression for the overall rate in eq 3 gives a sigmoidal dependence on pressure and reaches bimolecular pressure-independent limits at low and high pressures.[17] At 250 K, the rate of OH + HNO_3 in N_2 bath gas increased by ∼28% when the pressure increased from 20 to 200 Torr. If we extrapolate the low-pressure rate at 7 Torr from our previous report[11] and compare with the high-pressure data at 93 Torr at 249K, the increase in rate due to pressure is ∼47%. The doubly hydrogen-bonded OH−HNO_3 complex is calculated to be bound by 6.0 kcal mol^{-1} with respect to OH and HNO_3,[20] very similar to 6.5 kal mol^{-1} calculated for the CH_3COOH−OH complex.[10] The observed increase of rate due to the change in pressure is in line with the established OH + HNO_3 system. However, the OH + HNO_3 system does not have the two-channel feature seen in the title reaction. More experi-

ments at low temperatures ($T < 250$ K) and high pressures ($P > 100$ Torr) are needed to help understand the complete pressure and temperature effects on the OH + CH_3COOH reaction rate.

Atmospheric Implications. The main oxidation mechanism of acetic acid in the upper troposphere is via reaction with OH radicals. The major reaction channel, channel 1a, yields the methyl radical (CH_3), which under atmospheric conditions rapidly reacts with O_2 and forms methyl peroxy radical, shown in reaction 4. Oxidation of methane yields the methyl peroxy radical via a similar mechanism, as shown in reaction 5.

$$CH_3COOH + OH \rightarrow\rightarrow CH_3 + CO_2 + H_2O + (O_2) \rightarrow CH_3O_2 + CO_2 + H_2O \quad (4)$$

$$CH_4 + OH \rightarrow CH_3 + H_2O + (O_2) \rightarrow CH_3O_2 + H_2O \quad (5)$$

Extrapolating our Arrhenius expression obtained at 93 Torr to 220 K, a rate of 2.6×10^{-12} cm^3 $molecule^{-1}$ s^{-1} is obtained. This should be the lower limit for the rate since the actual pressure in the upper troposphere is higher than 93 Torr and would infer an even faster reaction rate. If we estimate the rate for the title reaction to be 3×10^{-12} cm^3 $molecule^{-1}$ s^{-1} in the upper troposphere, coupled with an observed acetic acid concentration as high as 2 ppbv,[3] it is possible to compare the production of the methyl peroxy radical by acetic acid oxidation and by methane oxidation. The factor of 0.66−1 indicates the uncertainty in the branching ratio for channel 1a and 1b.

$$k_{CH_3COOH}[CH_3COOH](0.66 - 1)/k_{CH_4}[CH_4] = (3 \times 10^{-12})(2)(0.66 - 1)/(8 \times 10^{-16})(1700) = 2.9 - 4.4 \quad (6)$$

The rate for methane + OH was calculated using the JPL-06 recommended value, and the 1700 ppbv is a rough average of observed methane concentration measured in TRACE A expedition.[3] In cases where the acetic acid concentration is present at the hundreds of pptv level,[21,22] the importance of acetic acid remains but the degree decreases.

Conclusions

We present our kinetics data of the reaction OH + CH_3COOH at 93 Torr from 241 to 301 K. The Arrhenius expression of $k(T) = (2.44 \pm 0.22) \times 10^{-14} \exp((1027 \pm 24)/T))$ is obtained. Comparison of our 93 Torr data set with the previously reported 7 Torr data set yields experimental evidence for a positive pressure dependence of the OH + CH_3COOH reaction rate for the first time. The observed pressure dependence supports a termolecular reaction mechanism and a PES calculated by De Smedt et al.[9] and Rosado-Reyes and Francisco[9,10] and is similar to the OH + HNO_3 system. Extrapolation of our Arrhenius expression to conditions representative of the upper troposphere and lower stratosphere yields a reaction rate constant higher than previously reported, making acetic acid as important as methane in controlling the oxidative capacity of the upper troposphere if acetic acid concentrations are high, though other oxygenates such as acetone are key players as well. More experimental data are needed at higher pressures and lower temperatures for this reaction.

Acknowledgment. The authors thank Dr. Jesse Kroll, Dr. David Wilmouth, and Dr. Mark Witinski for valuable discussions.

References and Notes

(1) Rigby, M.; Prinn, R. G.; Fraser, P. J.; Simmonds, P. G.; Langenfelds, R. L.; Huang, J.; Cunnold, D. M.; Steele, L. P.; Krummel, P. B.; Weiss, R. F.; O'Doherty, S.; Salameh, P. K.; Wang, H. J.; Harth, C. M.; Muhle, J.; Porter, L. W. *Geophys. Res. Lett.* **2008**, *35*, 6.

(2) Wennberg, P. O.; Hanisco, T. F.; Jaegle, L.; Jacob, D. J.; Hintsa, E. J.; Lanzendorf, E. J.; Anderson, J. G.; Gao, R. S.; Keim, E. R.; Donnelly, S. G.; Del Negro, L. A.; Fahey, D. W.; McKeen, S. A.; Salawitch, R. J.; Webster, C. R.; May, R. D.; Herman, R. L.; Proffitt, M. H.; Margitan, J. J.; Atlas, E. L.; Schauffler, S. M.; Flocke, F.; McElroy, C. T.; Bui, T. P. *Science* **1998**, *279*, 49.

(3) Jacob, D. J.; Heikes, B. G.; Fan, S. M.; Logan, J. A.; Mauzerall, D. L.; Bradshaw, J. D.; Singh, H. B.; Gregory, G. L.; Talbot, R. W.; Blake, D. R.; Sachse, G. W. *J. Geophys. Res.-Atmos.* **1996**, *101*, 24235.

(4) Dagaut, P.; Wallington, T. J.; Liu, R. Z.; Kurylo, M. J. *Int. J. Chem. Kinet.* **1988**, *20*, 331.

(5) Singleton, D. L.; Paraskevopoulos, G.; Irwin, R. S. *J. Am. Chem. Soc.* **1989**, *111*, 5248.

(6) Butkovskaya, N. I.; Kukui, A.; Pouvesle, N.; LeBras, G. *J. Phys. Chem. A* **2004**, *108*, 7021.

(7) Vimal, D.; Stevens, P. S. *J. Phys. Chem. A* **2006**, *110*, 11509.

(8) Khamaganov, V. G.; Bui, V. X.; Carl, S. A.; Peeters, J. *J. Phys. Chem. A* **2006**, *110*, 12852.

(9) De Smedt, F.; Bui, X. V.; Nguyen, T. L.; Peeters, J.; Vereecken, L. *J. Phys. Chem. A* **2005**, *109*, 2401.

(10) Rosado-Reyes, C. M.; Francisco, J. S. *J. Phys. Chem. A* **2006**, *110*, 4419.

(11) Huang, Y.-w.; Dransfield, T. J.; Miller, J. D.; Rojas, R. D.; Castillo, X. G.; Anderson, J. G. *J. Phys. Chem. A* **2009**, *113*, 423.

(12) Sun, W.; Saeys, M. *J. Phys. Chem. A* **2008**, *112*, 6918.

(13) Abbatt, J. P. D.; Demerjian, K. L.; Anderson, J. G. *J. Phys. Chem.* **1990**, *94*, 4566.

(14) Donahue, N. M.; Clarke, J. S.; Demerjian, K. L.; Anderson, J. G. *J. Phys. Chem.* **1996**, *100*, 5821.

(15) Donahue, N. M.; Dubey, M. K.; Mohrschladt, R.; Demerjian, K. L.; Anderson, J. G. *J. Geophys. Res.-Atmos* **1997**, *102*, 6159.

(16) Sprengnether, M. M.; Demerjian, K. L.; Dransfield, T. J.; Clarke, J. S.; Anderson, J. G.; Donahue, N. M. *J. Phys. Chem. A* **2009**, *113*, 5030.

(17) Brown, S. S.; Burkholder, J. B.; Talukdar, R. K.; Ravishankara, A. R. *J. Phys. Chem. A* **2001**, *105*, 1605.

(18) Brown, S. S.; Talukdar, R. K.; Ravishankara, A. R. *J. Phys. Chem. A* **1999**, *103*, 3031.

(19) Smith, I. W. M.; Ravishankara, A. R. *J. Phys. Chem. A* **2002**, *106*, 4798.

(20) Aloisio, S.; Francisco, J. S. *J. Phys. Chem. A* **1999**, *103*, 6049.

(21) Talbot, R. W.; Dibb, J. E.; Lefer, B. L.; Scheuer, E. M.; Bradshaw, J. D.; Sandholm, S. T.; Smyth, S.; Blake, D. R.; Blake, N. J.; Sachse, G. W.; Collins, J. E.; Gregory, G. L. *J. Geophys. Res.-Atmos.* **1997**, *102*, 28303.

(22) Reiner, T.; Mohler, O.; Arnold, F. *J. Geophys. Res.-Atmos.* **1999**, *104*, 13943.

JP106446Q